Journal Name

COMMUNICATION

A Report of Emergent Uranyl Binding Phenomena by an Amidoxime Phosphonic Acid Co-Polymer†

Received 00th January 20xx,
Accepted 00th January 20xx

DOI: 10.1039/x0xx00000x

www.rsc.org/

C.W. Abney,[a*] S. Das,[a] R. T. Mayes,[a] L.-J. Kuo,[b] J. Wood,[b] G. Gill,[b] M. Piechowicz,[c] Z. Lin,[c] W. Lin,[c] and S. Dai[a]

Development of technology to harvest the uranium dissolved in seawater would enable access to vast quantities of this critical metal for nuclear power generation. Amidoxime polymers are the most promising platform for achieving this separation, yet design of advanced adsorbents is hindered by uncertainty regarding the uranium binding mode. In this work we use XAFS to investigate the uranium coordination environment in an amidoxime-phosphonic acid copolymer adsorbent. In contrast to the binding mode predicted computationally and from small molecule studies, a cooperative chelating model is favoured, attributable to emergent behavior resulting from inclusion of amidoxime in a polymer. Samples exposed to seawater also display a feature consistent with a μ^2-oxo-bridged transition metal, suggesting formation of an *in situ* specific binding site. These findings challenge long held assumptions and provide new opportunities for the design of advanced adsorbent materials.

The extraction of uranium from seawater has been investigated since the 1950's,[1, 2] yet remains an unsolved chemical separation with potential "to change the world."[3] As the oceans contain more than 1000× the quantity of uranium available in terrestrial ores,[4] developing economical and efficient processes for harvesting this unconventional reserve would enable an effectively limitless supply of nuclear fuel for sustained power production and provide a financial backstop for stabilizing global uranium markets.[5] Amidoxime-functionalized adsorbents were initially investigated for this application more than three decades ago,[6, 7] yet remain the state-of-the-art technology having benefitted from developments in substrate engineering,[8] polymerization techniques,[9-11] and pre-deployment conditioning processes.[12] Despite recent increases in adsorption capacity, research efforts are hindered by a dearth of material characterization data, and therefore largely relegated to the systematic tuning of treatment parameters for optimizing performance, rather than developing fundamentally new adsorbents capable of transformative breakthroughs.

One particular science gap is the lack of direct information regarding the precise mode of uranium binding. Due to the exceptionally low concentration of uranium in seawater (3.3 μg L^{-1}), even the best performing adsorbents can only concentrate uranium to approximately 0.5 wt%, while competing metals such as Ca, Mg, and V, can each be up to 70× more abundant. Characteristic uranium signatures are below the limits of detection for observation by traditional spectroscopies, and non-specific x-ray scattering approaches are overwhelmed by the large quantities of competing metals.

Previous research has relied heavily upon small molecule investigations as well as computational approaches to predict the putative uranyl binding mode occurring on amorphous adsorbents. Early crystal structures reported monodentate binding of acetamidoxime and benzamidoxime to uranyl through the oxime oxygen (Figure 1, COJGIR),[13] while simultaneous reports from the groups of Hay[14] and Rogers[15] later indicated amidoxime binds uranyl in an η^2-fashion (*e.g.*, BARYUQ), strongly supported by related mononuclear uranyl-oxime crystal structures available in the literature.[16-25] The first instance of two adjacent amidoxime groups binding one uranyl was obtained with a 4,5-di(amidoxime) imidazole ligand, with both oximate moieties adopting an η^2-motif.[26] These results suggest such cooperative interactions may be achieved in polymer-based when binding sites are ideally oriented, as demonstrated previously through computational approaches.[27] Synthesis of amidoxime-functionalized adsorbents is traditionally achieved by polymerization of acrylonitrile, followed by treatment with hydroxylamine to generate the desired amidoxime group. This treatment process is also known to generate cyclic imide dioxime sites (TEVWAU) which have been ascribed with exceptional affinity for uranium

[a] *Oak Ridge National Laboratory, P.O. Box 2008, Oak Ridge, Tennessee 37831-6181, USA. E-mail: abneycw@ornl.gov*
[b] *Marine Sciences Laboratory, Pacific Northwest National Laboratory, Sequim, Washington 98382, USA.*
[c] *The University of Chicago, 929 East 57th Street, Chicago, Illinois 60637, USA.*

†Electronic Supplementary Information (ESI) available: general experimental details; adsorbent pre-treatment and brine/seawater-contact conditions; composition of uranium brine; ICP-OES/-AES analysis of metals on AI-8; XAFS data collection, processing, and fitting details; comparison of EXAFS data at different *k*-weights. See DOI: 10.1039/x0xx00000x

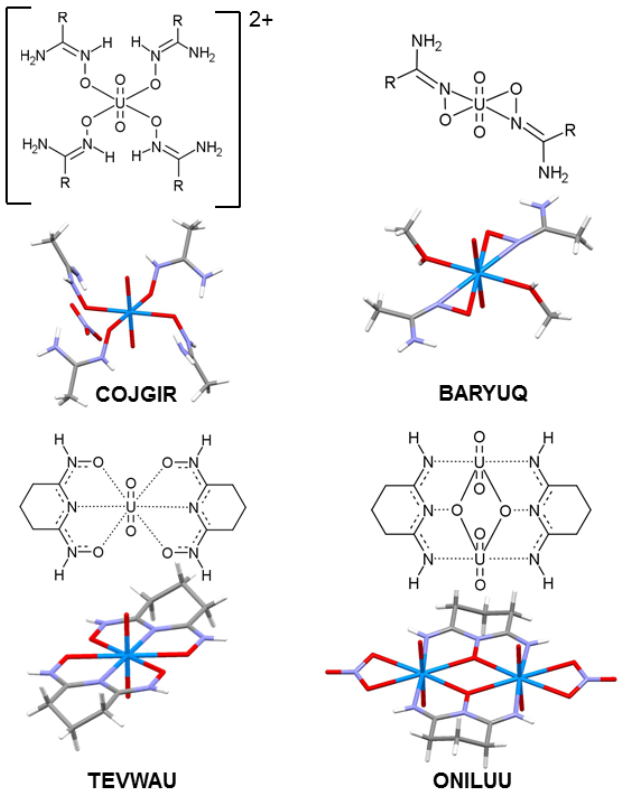

Figure 1. Crystal structures and chemical drawings for small molecule complexes used to investigate how amidoxime binds uranyl. CCDC identifiers are provided below the crystal structures. BARYOK, one of the crystalline standards used in this study, displays an identical uranium binding mode as BARYUQ, and differs only in the substitution of a phenyl for the methyl group on the ligand. BARYUQ is displayed for the sake of simplicity.

as well,[28-30] as demonstrated by rigorous titration experiments by Rao, *et. al.*[31-33] Finally, work by Warner and colleagues articulated the metal-catalyzed cyclization of two adjacent amidoximes on glutardiamidoxime to form 2,6-diiminopiperidin-1-ol, and the subsequent uranium binding and crystallization to form oxo-bridged dinuclear uranyl complexes (ONILUU).[34] Figure 1 displays representative crystal structures from the aforementioned small molecule studies.

Recently, we applied X-ray absorption fine structure (XAFS) spectroscopy to an adsorbent prepared by radiation-induced graft polymerization of polyacrylonitrile and itaconic acid on a polyethylene trunk material.[35] For samples exposed to brine solutions of either uranium or uranium and vanadium, fits of the extended XAFS (EXAFS) spectra were most consistent with two chelating amidoxime groups per uranyl, contesting the paradigm from previous small molecule studies. This model was supported through density functional theory (DFT) calculations performed at a high level of theory, following application of coupled cluster theory corrections. Differences in uranyl binding modes by a single amidoxime varied in energy by only 0 – 2 kcal mol^{-1}, and the thermodynamically preferred binding mode for two amidoximes included one bound in an η^2-fashion and the other chelating.[35] Furthermore, adsorbents deployed in environmental seawater displayed an entirely different binding motif than those contacted with the brine solutions, possessing an adjacent transition metal to form a μ^2-oxo-bridging species. Elegant work subsequently performed by Wu, Wang, and colleagues leveraged XAFS and DFT calculations to investigate the binding of $[UO_2(CO_3)_3]^{4-}$ by acetamidoxime *in situ*, concluding the amidoxime small molecule adopts the η^2-motif when not contained in a polymer.[36]

The divergent binding modes observed in the small molecule[36] and polymer systems[35] embodies the definition of emergent phenomena: macroscopic behaviour arising from interactions of molecules which individually do not display such properties. This effect was unanticipated, yet by influencing the uranyl binding mode this emergent behaviour is clearly a major contributor to the observed uranium uptake. Additional research is needed to determine whether such phenomena is an isolated anomaly unique only to the initial system investigated, or is similarly responsible for uranium binding in other related polymer-based systems. The ability to alter the metal binding mode by influencing mesoscale material structure would constitute an entirely novel approach to designing advanced adsorbents, and could have profound effects on the field of separations science.

In this work we apply XAFS to investigate the uranium binding mode for a different polymer adsorbent composed of poly(amidoxime-co-vinylphosphonic acid), colloquially referred to as AI-8.[10‡] Phosphates are well-known to bind actinide complexes, as has been abundantly established through decades of actinide partitioning processes,[37, 38] as well as for binding uranyl under acidic conditions with polymers,[39, 40] mesoporous silica,[41] mesoporous carbon,[42] and metal-organic frameworks.[43] While inclusion of vinylphosphonic acid as a comonomer has resulted in enhanced uranyl uptake compared with pure polyamidoxime, it is unknown whether this occurs through direct participation in uranyl binding or through induction of emergent behaviour in the adsorbent system, similar to that reported previously.[35]

AI-8 was synthesized as reported in the literature, with a molar comonomer ratio of 3.52:1 acrylonitrile to vinylphosphonic acid in the polymerization solution.[10] Controls displaying amidoxime η^2- and cyclic imide dioxime tridentate binding modes were prepared from small molecule crystals BARYOK (identical in binding mode to BARYUQ)[14] and TEVWAU,[31] displayed in Figure 1. A control adsorbent capable of only displaying phosphate binding was prepared identically to AI-8, but by not treating the poly(acrylonitrilie-co-vinylphosphonic acid) precursor with hydroxylamine, thereby never forming the amidoxime functionalities. A detailed synthetic protocol and characterization data for AI-8[10] and small molecule standards are available in the literature.[14, 31]

AI-8 adsorbent was contacted with an 8 ppm uranyl brine solution for 24 hours under agitation, while a second batch was deployed in filtered environmental seawater for 42 days at the Marine Sciences Laboratory of Pacific Northwest National Laboratory.[44, 45] This latter sample was subsequently split in half, with one half processed directly into a sample for XAFS

analysis and the other half contacted with 0.05 M HCl for elution of weakly-bound transition metals.

Dried polymer samples were prepared for XAFS analysis via cryogenic pulverization, then pressed without diluent into the centre of a Nylon flat washer, sealed with transparent "Scotch" tape, and encapsulated in a Mylar envelope. Data were collected at the uranium L_{III}-edge (17166 eV) on beamline 10-BM, B at the Advanced Photon Source of Argonne National Laboratory.[46] Data were processed using the Demeter software suite based on FEFF 6.[47, 48]

A qualitative comparison of the extended XAFS (EXAFS) data is particularly enlightening (Figure 2). In particular, characteristic differences are apparent between spectra collected on the two small molecule standards, as well as for both brine and seawater-contacted AI-8. The small molecule standard depicting the tridentate binding mode displays a bimodal feature at approximately 2 Å, and a broad feature at 3 Å.§ Previous work attributed these to scattering off the imine nitrogen and the 8 light scatterers (C, N, or O) composing the second coordination sphere, respectively.[35] In contrast, the standard possessing η^2-binding of uranyl is monomodal at 2 Å and displays no appreciable features farther in R-space. These results are representative of a single bond length for the first coordination sphere.

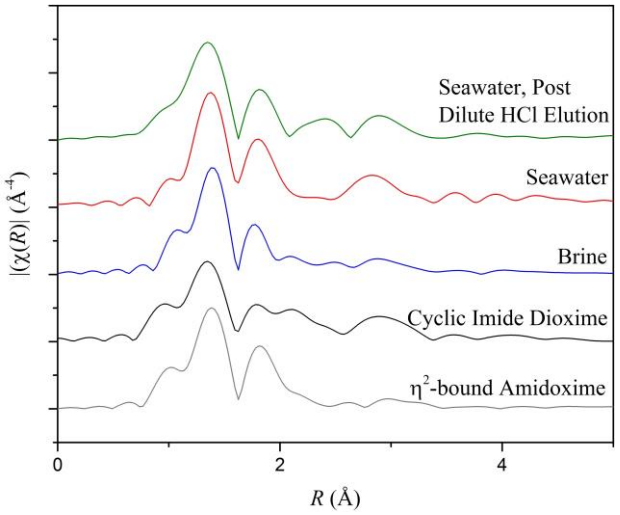

Figure 2. Direct comparison of uranium L_3-edge EXAFS spectra for small molecule standards and AI-8 exposed to brine or environmental seawater. Noteworthy characteristic spectroscopic features differentiating the cyclic imide dioxime include the 1:1 bimodal feature at 2 Å attributable to the imide nitrogen, and the broad feature at 3 Å from distant carbon and nitrogen. The bimodal feature is notably absent from the AI-8 spectra.

For the brine-contacted AI-8, the EXAFS spectrum appears to display features of both small molecule standards. Notably, close comparison with the cyclic imide dioxime spectrum suggests the possibility of contributions from a cyclic binding mode (Figure 3, right). Integrating the area under the peaks at 2 Å for the cyclic imide dioxime small molecule standard afforded an apparent 1:1 ratio, while the AI-8 adsorbent possessed a more modest 2.3:1 ratio, suggesting as much as 30% of the average uranyl coordination environment could be attributable to a cyclic binding mode.

Fitting the brine-contacted AI-8 was achieved through inclusion of three shells of variable numbers of light scatterers. The strongly-bound axial oxygen of uranyl (O_{yl}) comprise the first shell, with the coordination number fixed at 2. Three linear multiple scattering paths also correspond to these tightly-bound oxygen, and inclusion made a statistically significant improvement in the fits. The second shell, corresponding to the elements located in the uranyl equatorial plane, contains a variable number of O and N of two different path lengths, as well as a fixed contribution from the cyclic imine N discussed above. As the equatorial coordination environment of uranyl is known to be between 5 and 6,[14, 31, 49, 50] the sum of these nearest equatorial atoms was restrained to less than 6 during the fitting. The third and final shell, comprising the elements in the second coordination sphere, includes a variable number of N and C of three different path lengths. Inclusion of a carbonate scattering path was necessary to achieve statistically robust fits and thus provides the rationale for including a third path length. Importantly, no contributions from phosphate were necessary, despite vinyl phosphonic acid comprising a significant fraction of the polymer. Control experiments performed in brine with non-amidoximated AI-8, where only the phosphonic acid could potentially bind uranyl, displayed no quantifiable uranium uptake as determined by ICP-OES. This comonomer is thus considered innocent with regards to direct uranium binding, though its influence on polymer morphology and the effect on adsorbent performance merit further investigation.

Two reasonable models were able to successfully fit the brine-contacted AI-8 data. In the first, 30% of the ligation of uranyl was set as attributed to a cyclic binding site, as discussed above. In the second model, the cyclic contribution was a free parameter, restrained to less than 30% of uranyl ligation. In these instances, the contribution from the cyclic binding mode converged to 0 and was removed from the fit; this model is referred to as the "non-cyclic" model, for sake of simplicity. For the cyclic and non-cyclic models, the uranyl equatorial plane is formed from 6 ± 0.2 and 5.1 ± 1.2 light scatterers, respectively. The more distant scattering paths were fit by 2.8 ± 0.8 light scatterers and 0.7 ± 0.4 carbonates in the cyclic model, and 4.4 ± 1.6 light scatterers and 0.9 ± 0.7 carbonates in the non-cyclic model. Final parameters for both fits are provided in Table 1, with the fit from the non-cyclic model displayed in Figure 3. Models representative of an η^2-binding mode were attempted, but required a physically impossible number of amidoxime ligands bound to uranyl (> 4) in order to achieve an adequate fit of the data, and efforts to restrain the coordination environment to more reasonable values resulted in deterioration of the fit.

While both cyclic and non-cyclic models achieved sufficient *R*-factors (1.3 and 1.1, respectively), the non-cyclic model is superior from a purely statistical standpoint, particularly in light of the lower value for χ_ν^2 (59.4) compared to the cyclic model (70.0). Moreover, close inspection of the fitted parameters reveal the cyclic model possesses the maximum number of light scatterers permissible in the

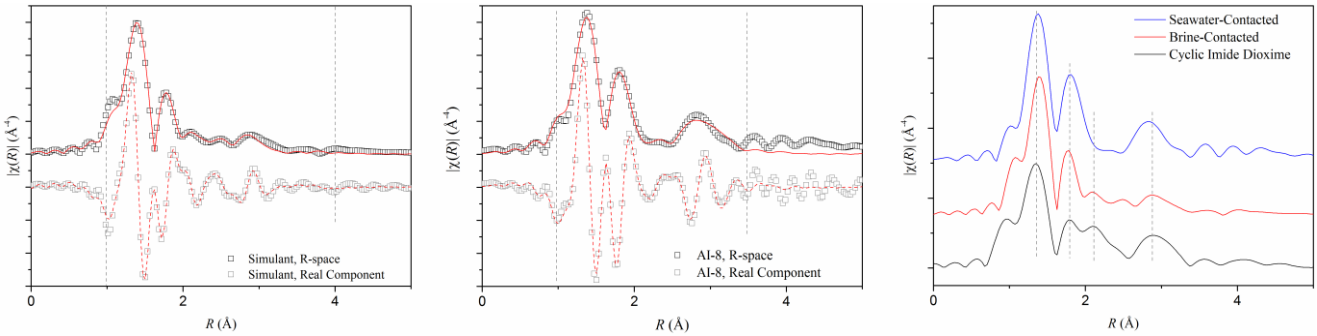

Figure 3. Data (squares) and fit (line) of AI-8 exposed to brine (left) and environmental seawater (centre). The lower plot is the real-space component of the Fourier transform, while the upper plot is the magnitude of the Fourier transform. The grey dashed lines represent the region over which the data were fitted. (Left) Fit of EXAFS spectra for Brine-contacted AI-8. (Centre) Fit of EXAFS spectra for seawater-contacted AI-8. (Right) Comparison of brine- and seawater-contacted AI-8 with the cyclic imide dioxime small molecule standard. Dashed grey lines are a guide for the eye for comparing location of peaks in spectra.

Table 1 EXAFS fits for cyclic and non-cyclic models for brine-contacted AI-8

Cyclic Model
(R = 1.38%, χ_v^2 = 70.0)

Path	Coord. No.[a.]	Bond Length (Å)	σ^2 ($\times 10^{-3}$ Å^2)
U→O_{yl}	2	1.82 ± 0.01	2 ± 0.3
U→O_1	2.7 ± 0.1	2.34 ± 0.02	8 ± 1
U→O_2	2.7 ± 0.1	2.44 ± 0.02	8 ± 1
U→N_{imide}	0.6	2.55 ± 0.03	2 ± 0.4
U→C_{CO3}	0.7 ± 0.4	2.91 ± 0.03	2 ± 0.4
U→N	1.4 ± 0.4	3.44 ± 0.03	2 ± 0.4
U→C	1.4 ± 0.4	3.34 ± 0.03	2 ± 0.4
U→$O_{yl(1)}$ →$O_{yl(2)}$	2	3.63 ± 0.01	4 ± 1
U→$O_{yl(1)}$ →U→$O_{yl(1)}$	2	3.63 ± 0.01	4 ± 1
U→$O_{yl(1)}$ →U→$O_{yl(2)}$	2	3.63 ± 0.01	4 ± 1

Non-Cyclic Model
(R = 1.10%, χ_v^2 = 59.4)

Path	Coord. No.[a.]	Bond Length (Å)	σ^2 ($\times 10^{-3}$ Å^2)
U→O_{yl}	2	1.81 ± 0.01	2 ± 0.2
U→N_{amine}	1.7 ± 0.4	2.49 ± 0.02	6 ± 2
U→O	3.4 ± 0.8	2.34 ± 0.02	6 ± 2
U→C_{CO3}	0.9 ± 0.7	2.92 ± 0.03	3 ± 3
U→N	2.2 ± 0.8	3.35 ± 0.02	3 ± 3
U→C	2.2 ± 0.2	3.47 ± 0.04	3 ± 3
U→$O_{yl(1)}$ →$O_{yl(2)}$	2	3.63 ± 0.01	4 ± 1
U→$O_{yl(1)}$ →U→$O_{yl(1)}$	2	3.63 ± 0.01	4 ± 1
U→$O_{yl(1)}$ →U→$O_{yl(2)}$	2	3.63 ± 0.01	4 ± 1

[a.] Values provided without accompanying error were fixed during the fit of the data

equatorial plane. Removal of this restraint converges to a fit requiring the physically improbable 6.9 ± 1.4 scatterers. From these statistical and physical considerations, we reject the cyclic model and propose the non-cyclic model most accurately portrays the average uranyl binding environment. The coordination numbers and bond lengths are consistent with the previously published XAFS results for a related polymer adsorbent,[35] and an average uranyl binding environment composed of 1.5 chelating amidoximes, 0.5 carbonates, and one aqua ligand is proposed. The chelating mode of amidoxime binding to uranyl has never been observed in small molecule studies due to being slightly thermodynamically less favourable than the η^2-binding mode.[14, 35] Excitingly, this result indicates a new uranium binding mode is activated by inclusion of amidoxime within a polymer, and is thus an instance of emergent phenomena resulting in different metal binding.

The seawater-contacted AI-8 was fit using the non-cyclic model developed from the brine-contacted adsorbent, with an equatorial coordination environment refined to 5.0 ± 0.6 light scatters. However, a significant feature is evident at 3 Å which cannot be fit through the non-cyclic model described above. When fit with only light scattering elements and P, a physically unreasonable number of atoms are necessary to model the feature. Comparison of the EXAFS data at different *k*-weighting (Figure S1, ESI†) reveals the feature at 3 Å increases as a function of *k*-weight, suggesting a heavier scattering element similar to that reported in previous work[35] and later suggested by Warner and colleagues.[34] Dinuclear uranyl-oxo Cu, Fe, Zn, and V complexes have all been reported in the literature,[51-57] and ICP-AES analysis of the seawater-contacted adsorbent reveal these elements are all present on the AI-8 adsorbent, with Fe and V in significantly greater molar quantities than uranium (Table S2, ESI†).

An analysis of the AI-8 treated with dilute HCl was attempted in an effort to confirm the origins of this feature. In contrast to prior work,[35] the HCl elution did not significantly suppress the feature at 3 Å (Figure 1), eliminating the possibility of a weakly-coordinating transition metal, and instead suggesting an oxo-bridged U, V, or Fe binding site. Unfortunately, HCl treatment also introduced a large feature at 2.5 Å which cannot be conclusively identified, and a reliable fit for this data was not obtained.

Inclusion of a U-Fe scattering path[52] of 3.53 Å yields a third shell containing 5.1 ± 0.6 light scatterers and 1.1 ± 0.7 Fe (Table 2), consistent with two chelating amidoximes and one

oxo-bridged metal. Similar results can also be obtained with Ni or Zn, but their elution with HCl suggests they could only be minor contributors.[35] The error obtained is not excessive for fitting coordination numbers, and is likely due to the averaging of scattering paths from multiple different metals convolving with contributions from carbonate and chelating amidoximes identified previously. This fit is substantiated by the small molecule work reported by Warner,[34] as the local coordination environment of uranium would afford an EXAFS spectrum seemingly composed of two chelating groups and an oxo-bridged metal. However, the bond lengths for the dinuclear uranyl cluster are longer than those observed in our XAFS spectrum and the brine-contacted AI-8 displayed no feature at 3 Å.

Table 2 EXAFS fits for seawater-contacted AI-8

Non-Cyclic Model with μ^2-oxo-Fe Scatterer
(R = 1.42%, χ_v^2 = 17.1)

Path	Coord. No.[a.]	Bond Length (Å)	σ^2 ($\times 10^{-3}$ Å^2)[a.]
U→O_{yl}	2	1.82 ± 0.01	2
U→O_1	2.5 ± 0.3	2.40 ± 0.02	2 ± 0.1
U→O_2	2.5 ± 0.3	2.53 ± 0.02	2 ± 0.1
U→N	2.6 ± 0.1	3.38 ± 0.02	2 ± 0.1
U→C	2.5 ± 0.1	3.37 ± 0.02	2 ± 0.1
U→O_1→N	5.1 ± 0.1	3.56 ± 0.03	2 ± 0.2
U→Fe	1.1 ± 0.7	3.52 ± 0.03	3 ± 2
U→$O_{yl(1)}$ →$O_{yl(2)}$	2	3.64 ± 0.01	4
U→$O_{yl(1)}$ →U→$O_{yl(1)}$	2	3.64 ± 0.01	4
U→$O_{yl(1)}$ →U→$O_{yl(2)}$	2	3.64 ± 0.01	4

[a.] Values provided without accompanying error were fixed during the fit of the data

Importantly, all efforts to fit the seawater-contacted AI-8 using models representative of an η^2- or cyclic binding mode were unsuccessful, regardless of inclusion of oxo-bridged transition metals, carbonate, or phosphate scattering paths. Consistent with our previous work[35] and previously reported chemical instability,[58] there is no direct evidence that supports tridentate binding through a cyclic imide dioxime functionality is responsible for coordinating uranyl in seawater.

Conclusions

A series of polymer adsorbents prepared by radiation induced graft polymerization were contacted with aqueous uranyl and investigated by XAFS to determine the uranium binding environment. In contrast to results from crystallographic,[14, 15, 26] computational,[14, 59] and *in situ* XAFS investigations using small molecule analogues,[36] amidoxime displays a distinctly different binding mode when incorporated into a polymer and is thus an example of an emergent phenomena which can only be induced when included as part of a larger system. Although seeming to possess spectral features indicative of tridentate binding, fitting the XAFS spectrum for a brine-contacted AI-8 adsorbent revealed including the cyclic imide dioxime binding site resulted in a fit which was physically suspicious and less statistically rigorous than fits performed without the cyclic binding site. The seawater-contacted AI-8 displayed a large feature at 3 Å, similar to a related adsorbent investigated previously,[35] but in contrast to earlier results, the persistence of the peak following treatment with dilute HCl suggests the transition metal is strongly bound by the fibre, with Fe proposed as the oxo-bridged species.

Beyond simply identifying the uranium binding environments on this adsorbents, these results provide an important example of emergent behaviour and constitute a critical starting point for subsequent studies in this developing field of research. Emergent phenomena have been reported in a wide number of systems, ranging from formation of hierarchical calcium carbonate structures,[60] to viscoelasticity of branched and entangled polymers,[61] to the self-assembly of polymer-grafted nanoparticles[62] and polymer capsules.[63] However, to the best of our knowledge, amidoxime adsorbents constitute the first instance where the metal binding environment is directly affected by integration within a polymer. Due to the tunability of the polymer formulation, these materials are amenable to further investigation regarding the onset and persistence of emergent behaviour, and are expected to afford critical knowledge for the rational design of advanced materials with enhanced performance for selective metal ion separations.

Acknowledgements

This research was conducted at Oak Ridge National Laboratory (ORNL), the Marine Sciences Laboratory of Pacific Northwest National Laboratory (PNNL), and the University of Chicago. Work at ORNL and PNNL was sponsored by the U.S. Department of Energy (DOE), Office of Nuclear Energy. Work at the University of Chicago was supported by the U.S DOE Office of Nuclear Energy's Nuclear Energy University Program (Sub-Contract – 20 #120427, Project #3151).

XAFS data were collected at the Advanced Photon Source at Argonne National Laboratory on Beamline 10BM-B, supported by the Materials Research Collaborative Access Team (MRCAT). MRCAT operations are supported by the DOE and the MRCAT member institutions. The Advanced Photon Source is a U.S. DOE Office of Science User Facility operated for the DOE Office of Science by Argonne National Laboratory under Contract No. DE-AC02-06CH11357.

Notes and References

‡ The adsorbent formulation referred to as AI-8 in this work is denoted as AI-11 in the cited publication.

§ The EXAFS signal depends on $\sin[2kR_i + \delta_i(k)]$, where k is the energy of the photoelectron in wavenumbers, R is the half-path length of the i-th scatterer, and $\delta_i(k)$ is the phase shift of the photoelectron. In this work, we refer to the crystallographic positions of the atoms in terms of their actual distance in Å from uranium. However, their contributions to the Fourier transform of the data are discussed in terms of their distance in Å, uncorrected for $\delta_i(k)$. As a result, the plots of the Fourier transform display features attributable to atoms which are approximately 0.5 Å farther away than is indicated by the x-axis. Thus, half-path lengths (*i.e.*, bond lengths) of approximately 3.5 Å are most reasonable for generating a feature at 3 Å in *R*-space.

1. R. J. W. Streeton, *Continuous Extraction of Uranium from Sea Water*, Report AB 15/2806, UK National Archives, Atomic Energy Research Establishment, Harwell, 1953.
2. *The extraction of uranium from the sea (Oyster Project)*, Report AB 6/1264, UK National Archives, Atomic Energy Research Establishment, Harwell 1956-1961.
3. D. S. Sholl and R. P. Lively, *Nature*, 2016, **532**, 435-437.
4. J. Kim, C. Tsouris, R. T. Mayes, Y. Oyola, T. Saito, C. J. Janke, S. Dai, E. Schneider and D. Sachde, *Sep. Sci. Technol.*, 2013, **48**, 367-387.
5. H. Lindner and E. Schneider, *Energy Economics*, 2015, **49**, 9-22.
6. C. K. Nitta, F. R. Best and M. J. Driscoll, *Delayed Neutron Assay to Test Sorbers for Uranium-From-Seawater Applications*, Massachusetts Institute of Technology, Cambridge, Massachusetts (U.S.A.), 1982.
7. H. J. Schenk, L. Astheimer, E. G. Witte and K. Schwochau, *Sep. Sci. Technol.*, 1982, **17**, 1293-1308.
8. H.-B. Pan, W. Liao, C. M. Wai, Y. Oyola, C. J. Janke, G. Tian and L. Rao, *Dalton. Trans.*, 2014, **43**, 10713-10718.
9. T. Saito, S. Brown, S. Chatterjee, J. Kim, C. Tsouris, R. T. Mayes, L.-J. Kuo, G. Gill, Y. Oyola, C. J. Janke and S. Dai, *J. Mater. Chem. A*, 2014, **2**, 14674-14681.
10. S. Das, Y. Oyola, R. T. Mayes, C. J. Janke, L. J. Kuo, G. Gill, J. R. Wood and S. Dai, *Ind. Eng. Chem. Res.*, 2016, **55**, 4103-4109.
11. S. Das, Y. Oyola, R. T. Mayes, C. J. Janke, L. J. Kuo, G. Gill, J. R. Wood and S. Dai, *Ind. Eng. Chem. Res.*, 2015, DOI: 10.1021/acs.iecr.5b03136.
12. S. Das, W. P. Liao, M. Flicker Byers, C. Tsouris, C. J. Janke, R. T. Mayes, E. Schneider, L. J. Kuo, J. R. Wood, G. A. Gill and S. Dai, *Ind. Eng. Chem. Res.*, 2016, **55**, 4303-4312.
13. E. G. Witte, K. S. Schwochau, G. Henkel and B. Krebs, *Inorg. Chim. Acta*, 1984, **94**, 323-331.
14. S. Vukovic, L. A. Watson, S. O. Kang, R. Custelcean and B. P. Hay, *Inorg. Chem.*, 2012, **51**, 3855-3859.
15. P. S. Barber, S. P. Kelley and R. D. Rogers, *RSC. Adv.*, 2012, **2**, 8526-8530.
16. R. N. Shchelokov, Y. N. Mikhailov, A. G. Beirakhov, I. M. Orlova and Z. R. Ashurov, *Russ. J. Inorg. Chem.*, 1986, **31**, 2050.
17. R. Graziani, U. Casellato, P. A. Vigato, S. Tamburini and M. Vidali, *J. Chem. Soc., Dalton Trans.*, 1983, 697-701.
18. R. N. Shchelokov, Y. N. Mikhailov, A. G. Beirakhov, I. M. Orlova and Z. R. Ashurov, *Russ. J. Inorg. Chem.*, 1986, **31**, 2339.
19. R. N. Shchelokov, Y. N. Mikhailov, A. G. Beirakhov, I. M. Orlova and G. M. Lobanova, *Russ. J. Inorg. Chem.*, 1987, **32**, 1173.
20. A. G. Beirakhov, I. M. Orlova, Z. R. Ashurov, G. M. Lobanova, Y. N. Mikhailov and R. N. Schchelokov, *Russ. J. Inorg. Chem.*, 1990, **35**, 3139.
21. A. G. Beirakhov, I. M. Orlova, Z. R. Ashurov, G. M. Lobanova, Y. N. Mikhailov and R. N. Shchelokov, *Russ. J. Inorg. Chem.*, 1991, **36**, 647.
22. A. G. Beirakhov, I. M. Orlova, E. G. Ilyin, L. V. Goeva, A. V. Churakov, G. G. Aleksandrov, M. D. Surazhskaya and Y. N. Mikhailov, *Russ. J. Inorg. Chem.*, 2014, **59**, 1671.
23. A. G. Beirakhov, I. M. Orlova, E. G. Il'in, Y. E. Gorbunova and Y. N. Mikhailov, *Russ. J. Inorg. Chem.*, 2007, **52**, 2011.
24. A. G. Beirakhov, I. M. Orlova, E. G. Il'in, Y. E. Gorbunova and Y. N. Mikhailov, *Russ. J. Inorg. Chem.*, 2007, **52**, 39.
25. A. G. Beirakhov, I. M. Orlova, E. G. Il'in, A. V. Churakov, A. S. Kanishcheva and Y. N. Mikhailov, *Russ. J. Inorg. Chem.*, 2009, **54**, 1282.
26. S. P. Kelley, P. S. Barber, P. H. K. Mullins and R. D. Rogers, *Chem. Commun.*, 2014, **50**, 12504-12507.
27. S. Vukovic and B. P. Hay, *Inorg. Chem.*, 2013, **52**, 7805-7810.
28. L. Astheimer, H. J. Schenk, E. G. Witte and K. Schwochau, *Sep. Sci. Technol.*, 1983, **18**, 307-339.
29. Y. Kobuke, H. Tanaka and H. Ogoshi, *Polym J*, 1990, **22**, 179-182.
30. S. Das, S. Brown, R. T. Mayes, C. J. Janke, C. Tsouris, L. J. Kuo, G. Gill and S. Dai, *Chem. Eng. J.*, 2016, **298**, 125-135.
31. G. Tian, S. Teat, Z. Zhang and L. Rao, *Dalton. Trans.*, 2012, **41**, 11579-11586.
32. G. Tian, S. Teat and L. Rao, *Dalton. Trans.*, 2013, **42**, 5690-5696.
33. F. Endrizzi, A. Melchior, M. Tolazzi and L. Rao, *Dalton. Trans.*, 2015, **44**, 13835-13844.
34. Z. C. Kennedy, A. J. P. Cardenas, J. F. Corbey and M. G. Warner, *Chem. Commun.*, 2016, DOI: 10.1039/C6CC02488B.
35. C. W. Abney, R. T. Mayes, M. Piechowicz, Z. Lin, V. Bryantsev, G. M. Veith, S. Dai and W. Lin, *Energy Environ. Sci.*, 2016, **9**, 448-453.
36. L. Zhang, J. Su, S. Yang, X. Guo, Y. Jia, N. Chen, J. Zhou, S. Zhang, S. Wang, J. Li, J. Li, G. Wu and J.-Q. Wang, *Ind. Eng. Chem. Res.*, 2016, **55**, 4224-4230.
37. J. N. Mathur, M. S. Murali and K. L. Nash, *Solvent Extr. Ion Exch.*, 2001, **19**, 357-390.
38. M. Nilsson and K. L. Nash, *Solvent Extr. Ion Exch.*, 2007, **25**, 665-701.
39. S. D. Alexandratos and X. Zhu, *Sep. Sci. Technol.*, 2008, **43**, 1296-1309.
40. X. Zhu and S. D. Alexandratos, *Chem. Eng. Sci.*, 2015, **127**, 126-132.
41. J. L. Vivero-Escoto, M. Carboni, C. W. Abney, K. E. deKrafft and W. Lin, *Microporous Mesoporous Mater.*, 2013, **180**, 22-31.
42. M. Carboni, C. W. Abney, K. M. L. Taylor-Pashow, J. L. Vivero-Escoto and W. Lin, *Ind. Eng. Chem. Res.*, 2013, **52**, 15187-15197.
43. M. Carboni, C. W. Abney, S. Liu and W. Lin, *Chem. Sci.*, 2013, **4**, 2396-2402.
44. J. Kim, C. Tsouris, Y. Oyola, C. J. Janke, R. T. Mayes, S. Dai, G. Gill, L.-J. Kuo, J. Wood, K.-Y. Choe, E. Schneider and H. Lindner, *Ind. Eng. Chem. Res.*, 2014, **53**, 6076-6083.
45. J. Park, G. A. Gill, J. E. Strivens, L.-J. Kuo, R. T. Jeters, A. Avila, J. R. Wood, N. J. Schlafer, C. J. Janke, E. A. Miller, M. Thomas, R. S. Addleman and G. T. Bonheyo, *Ind. Eng. Chem. Res.*, 2016, **55**, 4328-4338.
46. A. J. Kropf, J. Katsoudas, S. Chattopadhyay, T. Shibata, E. A. Lang, V. N. Zyryanov, B. Ravel, K. McIvor, K. M. Kemner, K. G. Scheckel, S. R. Bare, J. Terry, S. D. Kelly, B. A. Bunker and C. U. Segre, *AIP Conf. Proc.*, 2010, **1234**, 299-302.

47. B. Ravel and M. Newville, *J. Synchrotron Radiat.*, 2005, **12**, 537-541.
48. J. J. Rehr and R. C. Albers, *Rev. Mod. Phys.*, 2000, **72**, 621-654.
49. P. G. Allen, J. J. Bucher, D. K. Shuh, N. M. Edelstein and T. Reich, *Inorg. Chem.*, 1997, **36**, 4676-4683.
50. S. D. Kelly, K. M. Kemner and S. C. Brooks, *Geochim. Cosmochim. Acta*, 2007, **71**, 821-834.
51. L. Mandal, S. Bhattacharya and S. Mohanta, *Inorg. Chim. Acta*, 2013, **406**, 87-94.
52. M. Basile, D. K. Unruh, E. Flores, A. Johns and T. Z. Forbes, *Dalton. Trans.*, 2015, **44**, 2597-2605.
53. L. Salmon, P. Thuery and M. Ephritikhine, *Journal*, 2006.
54. Ajay K. Sah, Chebrolu P. Rao, Pauli K. Saarenketo, Elina K. Wegelius, E. Kolehmainen and K. Rissanen, *Eur. J. Inorg. Chem.*, 2001, **2001**, 2773-2781.
55. D. L. Perry, H. Ruben, D. H. Templeton and A. Zalkin, *Inorg. Chem.*, 1980, **19**, 1067-1069.
56. L. Jouffret, M. Rivenet and F. Abraham, *J. Solid State Chem.*, 2010, **183**, 84-92.
57. G. A. Senchyk, E. M. Wylie, S. Prizio, J. E. S. Szymanowski, G. E. Sigmon and P. C. Burns, *Chem. Commun.*, 2015, **51**, 10134-10137.
58. S. O. Kang, S. Vukovic, R. Custelcean and B. P. Hay, *Ind. Eng. Chem. Res.*, 2012, **51**, 6619-6624.
59. C. W. Abney, S. Liu and W. Lin, *J. Phys. Chem. A*, 2013, **117**, 11558-11565.
60. X.-H. Guo, A.-W. Xu and S.-H. Yu, *Cryst. Growth Des.*, 2008, **8**, 1233-1242.
61. D. J. Read, D. Auhl, C. Das, J. den Doelder, M. Kapnistos, I. Vittorias and T. C. B. McLeish, *Science*, 2011, **333**, 1871-1874.
62. P. Akcora, H. Liu, S. K. Kumar, J. Moll, Y. Li, B. C. Benicewicz, L. S. Schadler, D. Acehan, A. Z. Panagiotopoulos, V. Pryamitsyn, V. Ganesan, J. Ilavsky, P. Thiyagarajan, R. H. Colby and J. F. Douglas, *Nat. Mater.*, 2009, **8**, 354-359.
63. R. K. Castellano, R. Clark, S. L. Craig, C. Nuckolls and J. Rebek, *Proc. Natl. Acad. Sci.*, 2000, **97**, 12418-12421.